Observation and study of the decay $J/\psi \to \phi\eta\eta'$

M. Ablikim,[1] M. N. Achasov,[10,d] S. Ahmed,[15] M. Albrecht,[4] M. Alekseev,[56a,56c] A. Amoroso,[56a,56c] F. F. An,[1] Q. An,[53,43] J. Z. Bai,[1] Y. Bai,[42] O. Bakina,[27] R. Baldini Ferroli,[23a] Y. Ban,[35,l] K. Begzsuren,[25] D. W. Bennett,[22] J. V. Bennett,[5] N. Berger,[26] M. Bertani,[23a] D. Bettoni,[24a] F. Bianchi,[56a,56c] E. Boger,[27,b] I. Boyko,[27] R. A. Briere,[5] H. Cai,[58] X. Cai,[1,43] O. Cakir,[46a] A. Calcaterra,[23a] G. F. Cao,[1,47] S. A. Cetin,[46b] J. Chai,[56c] J. F. Chang,[1,43] G. Chelkov,[27,b,c] G. Chen,[1] H. S. Chen,[1,47] J. C. Chen,[1] M. L. Chen,[1,43] P. L. Chen,[54] S. J. Chen,[33] X. R. Chen,[30] Y. B. Chen,[1,43] W. Cheng,[56c] X. K. Chu,[35,l] G. Cibinetto,[24a] F. Cossio,[56c] H. L. Dai,[1,43] J. P. Dai,[38,h] A. Dbeyssi,[15] D. Dedovich,[27] Z. Y. Deng,[1] A. Denig,[26] I. Denysenko,[27] M. Destefanis,[56a,56c] F. De Mori,[56a,56c] Y. Ding,[31] C. Dong,[34] J. Dong,[1,43] L. Y. Dong,[1,47] M. Y. Dong,[1,43,47] Z. L. Dou,[33] S. X. Du,[61] P. F. Duan,[1] J. Fang,[1,43] S. S. Fang,[1,47] Y. Fang,[1] R. Farinelli,[24a,24b] L. Fava,[56b,56c] S. Fegan,[26] F. Feldbauer,[4] G. Felici,[23a] C. Q. Feng,[53,43] E. Fioravanti,[24a] M. Fritsch,[4] C. D. Fu,[1] Q. Gao,[1] X. L. Gao,[53,43] Y. Gao,[45] Y. G. Gao,[6] Z. Gao,[53,43] B. Garillon,[26] I. Garzia,[24a] A. Gilman,[50] K. Goetzen,[11] L. Gong,[34] W. X. Gong,[1,43] W. Gradl,[26] M. Greco,[56a,56c] M. H. Gu,[1,43] Y. T. Gu,[13] A. Q. Guo,[1] R. P. Guo,[1,47] Y. P. Guo,[26] A. Guskov,[27] Z. Haddadi,[29] S. Han,[58] X. Q. Hao,[16] F. A. Harris,[48] K. L. He,[1,47] X. Q. He,[52] F. H. Heinsius,[4] T. Held,[4] Y. K. Heng,[1,43,47] Z. L. Hou,[1] H. M. Hu,[1,47] J. F. Hu,[38,h] T. Hu,[1,43,47] Y. Hu,[1] G. S. Huang,[53,43] J. S. Huang,[16] X. T. Huang,[37] X. Z. Huang,[33] Z. L. Huang,[31] T. Hussain,[55] W. Ikegami Andersson,[57] M. Irshad,[53,43] Q. Ji,[1] Q. P. Ji,[16] X. B. Ji,[1,47] X. L. Ji,[1,43] X. S. Jiang,[1,43,47] X. Y. Jiang,[34] J. B. Jiao,[37] Z. Jiao,[18] D. P. Jin,[1,43,47] S. Jin,[1,47] Y. Jin,[49] T. Johansson,[57] A. Julin,[50] N. Kalantar-Nayestanaki,[29] X. S. Kang,[34] M. Kavatsyuk,[29] B. C. Ke,[1] I. K. Keshk,[4] T. Khan,[53,43] A. Khoukaz,[51] P. Kiese,[26] R. Kiuchi,[1] R. Kliemt,[11] L. Koch,[28] O. B. Kolcu,[46b,f] B. Kopf,[4] M. Kornicer,[48] M. Kuemmel,[4] M. Kuessner,[4] A. Kupsc,[57] M. Kurth,[1] W. Kühn,[28] J. S. Lange,[28] P. Larin,[15] L. Lavezzi,[56c] H. Leithoff,[26] C. Li,[57] Cheng Li,[53,43] D. M. Li,[61] F. Li,[1,43] F. Y. Li,[35,l] G. Li,[1] H. B. Li,[1,47] H. J. Li,[1,47] J. C. Li,[1] J. W. Li,[41] Jin Li,[36] K. J. Li,[44] Kang Li,[14] Ke Li,[1] Lei Li,[3] P. L. Li,[53,43] P. R. Li,[47,7] Q. Y. Li,[37] W. D. Li,[1,47] W. G. Li,[1] X. L. Li,[37] X. N. Li,[1,43] X. Q. Li,[34] Z. B. Li,[44] H. Liang,[53,43] Y. F. Liang,[40] Y. T. Liang,[28] G. R. Liao,[12] L. Z. Liao,[1,47] J. Libby,[21] C. X. Lin,[44] D. X. Lin,[15] B. Liu,[38,h] B. J. Liu,[1] C. X. Liu,[1] D. Liu,[53,43] D. Y. Liu,[38,h] F. H. Liu,[39] Fang Liu,[1] Feng Liu,[6] H. B. Liu,[13] H. L. Liu,[42] H. M. Liu,[1,47] Huanhuan Liu,[1] Huihui Liu,[17] J. B. Liu,[53,43] J. Y. Liu,[1,47] K. Liu,[45] K. Y. Liu,[31] Ke Liu,[6] L. D. Liu,[35,l] Q. Liu,[47] S. B. Liu,[53,43] X. Liu,[30] Y. B. Liu,[34] Z. A. Liu,[1,43,47] Zhiqing Liu,[26] Y. F. Long,[35,l,*] X. C. Lou,[1,43,47] H. J. Lu,[18] J. G. Lu,[1,43] Y. Lu,[1] Y. P. Lu,[1,43] C. L. Luo,[32] M. X. Luo,[60] T. Luo,[9,j] X. L. Luo,[1,43] S. Lusso,[56c] X. R. Lyu,[47] F. C. Ma,[31] H. L. Ma,[1] L. L. Ma,[37] M. M. Ma,[1,47] Q. M. Ma,[1] T. Ma,[1] X. N. Ma,[34] X. Y. Ma,[1,43] Y. M. Ma,[37] F. E. Maas,[15] M. Maggiora,[56a,56c] S. Maldaner,[26] Q. A. Malik,[55] A. Mangoni,[23b] Y. J. Mao,[35,l] Z. P. Mao,[1] S. Marcello,[56a,56c] Z. X. Meng,[49] J. G. Messchendorp,[29] G. Mezzadri,[24b] J. Min,[1,43] R. E. Mitchell,[22] X. H. Mo,[1,43,47] Y. J. Mo,[6] C. Morales Morales,[15] N. Yu. Muchnoi,[10,d] H. Muramatsu,[50] A. Mustafa,[4] Y. Nefedov,[27] F. Nerling,[11] I. B. Nikolaev,[10,d] Z. Ning,[1,43] S. Nisar,[8] S. L. Niu,[1,43] X. Y. Niu,[1,47] S. L. Olsen,[36,k] Q. Ouyang,[1,43,47] S. Pacetti,[23b] Y. Pan,[53,43] M. Papenbrock,[57] P. Patteri,[23a] M. Pelizaeus,[4] J. Pellegrino,[56a,56c] H. P. Peng,[53,43] Z. Y. Peng,[13] K. Peters,[11,g] J. Pettersson,[57] J. L. Ping,[32] R. G. Ping,[1,47] A. Pitka,[4] R. Poling,[50] V. Prasad,[53,43] H. R. Qi,[2] M. Qi,[33] T. Y. Qi,[2] S. Qian,[1,43] C. F. Qiao,[47] N. Qin,[58] X. S. Qin,[4] Z. H. Qin,[1,43] J. F. Qiu,[1] S. Q. Qu,[34] K. H. Rashid,[55,i] C. F. Redmer,[26] M. Richter,[4] M. Ripka,[26] A. Rivetti,[56c] M. Rolo,[56c] G. Rong,[1,47] Ch. Rosner,[15] A. Sarantsev,[27,e] M. Savrié,[24b] K. Schoenning,[57] W. Shan,[19] X. Y. Shan,[53,43] M. Shao,[53,43] C. P. Shen,[2] P. X. Shen,[34] X. Y. Shen,[1,47] H. Y. Sheng,[1] X. Shi,[1,43] J. J. Song,[37] W. M. Song,[37] X. Y. Song,[1] S. Sosio,[56a,56c] C. Sowa,[4] S. Spataro,[56a,56c] G. X. Sun,[1] J. F. Sun,[16] L. Sun,[58] S. S. Sun,[1,47] X. H. Sun,[1] Y. J. Sun,[53,43] Y. K. Sun,[53,43] Y. Z. Sun,[1] Z. J. Sun,[1,43] Z. T. Sun,[22] Y. T. Tan,[53,43] C. J. Tang,[40] G. Y. Tang,[1] X. Tang,[1] I. Tapan,[46c] M. Tiemens,[29] B. Tsednee,[25] I. Uman,[46d] B. Wang,[1] B. L. Wang,[47] D. Wang,[35,l] D. Y. Wang,[35,l] Dan Wang,[47] K. Wang,[1,43] L. L. Wang,[1] L. S. Wang,[1] M. Wang,[37] Meng Wang,[1,47] P. Wang,[1] P. L. Wang,[1] W. P. Wang,[53,43] X. F. Wang,[45] X. L. Wang,[9,j] Y. Wang,[53,43] Y. F. Wang,[1,43,47] Z. Wang,[1,43] Z. G. Wang,[1,43] Z. Y. Wang,[1] Zongyuan Wang,[1,47] T. Weber,[4] D. H. Wei,[12] P. Weidenkaff,[26] S. P. Wen,[1] U. Wiedner,[4] M. Wolke,[57] L. H. Wu,[1] L. J. Wu,[1,47] Z. Wu,[1,43] L. Xia,[53,43] Y. Xia,[20] D. Xiao,[1] Y. J. Xiao,[1,47] Z. J. Xiao,[32] Y. G. Xie,[1,43] Y. H. Xie,[6] X. A. Xiong,[1,47] Q. L. Xiu,[1,43] G. F. Xu,[1] J. J. Xu,[1,47] L. Xu,[1] Q. J. Xu,[14] Q. N. Xu,[47] X. P. Xu,[41] F. Yan,[54] L. Yan,[56a,56c] W. B. Yan,[53,43] W. C. Yan,[2] Y. H. Yan,[20] H. J. Yang,[38,h] H. X. Yang,[1] L. Yang,[58] R. X. Yang,[53,43] Y. H. Yang,[33] Y. X. Yang,[12] Yifan Yang,[1,47] Z. Q. Yang,[20] M. Ye,[1,43] M. H. Ye,[7] J. H. Yin,[1] Z. Y. You,[44] B. X. Yu,[1,43,47] C. X. Yu,[34] J. S. Yu,[20] J. S. Yu,[30] C. Z. Yuan,[1,47] Y. Yuan,[1] A. Yuncu,[46b,a] A. A. Zafar,[55] Y. Zeng,[20] B. X. Zhang,[1] B. Y. Zhang,[1,43] C. C. Zhang,[1] D. H. Zhang,[1] H. H. Zhang,[44] H. Y. Zhang,[1,43] J. Zhang,[1,47] J. L. Zhang,[59] J. Q. Zhang,[4] J. W. Zhang,[1,43,47] J. Y. Zhang,[1] J. Z. Zhang,[1,47] K. Zhang,[1,47] L. Zhang,[45] T. J. Zhang,[38,h] X. Y. Zhang,[37] Y. Zhang,[53,43] Y. H. Zhang,[1,43] Y. T. Zhang,[53,43] Yang Zhang,[1] Yao Zhang,[1] Yi Zhang,[9,j] Yu Zhang,[47] Z. H. Zhang,[6] Z. P. Zhang,[53] Z. Y. Zhang,[58] G. Zhao,[1] J. W. Zhao,[1,43] J. Y. Zhao,[1,47] J. Z. Zhao,[1,43] Lei Zhao,[53,43] Ling Zhao,[1] M. G. Zhao,[34] Q. Zhao,[1] S. J. Zhao,[61] T. C. Zhao,[1] Y. B. Zhao,[1,43] Z. G. Zhao,[53,43] A. Zhemchugov,[27,b] B. Zheng,[54] J. P. Zheng,[1,43] Y. H. Zheng,[47] B. Zhong,[32] L. Zhou,[1,43] Q. Zhou,[1,47] X. Zhou,[58] X. K. Zhou,[53,43] X. R. Zhou,[53,43] X. Y. Zhou,[1] Xiaoyu Zhou,[20] Xu Zhou,[20] A. N. Zhu,[1,47] J. Zhu,[34] J. Zhu,[44] K. Zhu,[1] K. J. Zhu,[1,43,47] S. Zhu,[1] S. H. Zhu,[52] X. L. Zhu,[45] Y. C. Zhu,[53,43] Y. S. Zhu,[1,47] Z. A. Zhu,[1,47] J. Zhuang,[1,43] B. S. Zou,[1] and J. H. Zou,[1]

(BESIII Collaboration)

[1]Institute of High Energy Physics, Beijing 100049, People's Republic of China
[2]Beihang University, Beijing 100191, People's Republic of China
[3]Beijing Institute of Petrochemical Technology, Beijing 102617, People's Republic of China
[4]Bochum Ruhr-University, D-44780 Bochum, Germany
[5]Carnegie Mellon University, Pittsburgh, Pennsylvania 15213, USA
[6]Central China Normal University, Wuhan 430079, People's Republic of China
[7]China Center of Advanced Science and Technology, Beijing 100190, People's Republic of China
[8]COMSATS Institute of Information Technology,
Lahore, Defence Road, Off Raiwind Road, 54000 Lahore, Pakistan
[9]Fudan University, Shanghai 200443, People's Republic of China
[10]G.I. Budker Institute of Nuclear Physics SB RAS (BINP), Novosibirsk 630090, Russia
[11]GSI Helmholtzcentre for Heavy Ion Research GmbH, D-64291 Darmstadt, Germany
[12]Guangxi Normal University, Guilin 541004, People's Republic of China
[13]Guangxi University, Nanning 530004, People's Republic of China
[14]Hangzhou Normal University, Hangzhou 310036, People's Republic of China
[15]Helmholtz Institute Mainz, Johann-Joachim-Becher-Weg 45, D-55099 Mainz, Germany
[16]Henan Normal University, Xinxiang 453007, People's Republic of China
[17]Henan University of Science and Technology, Luoyang 471003, People's Republic of China
[18]Huangshan College, Huangshan 245000, People's Republic of China
[19]Hunan Normal University, Changsha 410081, People's Republic of China
[20]Hunan University, Changsha 410082, People's Republic of China
[21]Indian Institute of Technology Madras, Chennai 600036, India
[22]Indiana University, Bloomington, Indiana 47405, USA
[23a]INFN Laboratori Nazionali di Frascati, I-00044, Frascati, Italy
[23b]INFN and University of Perugia, I-06100, Perugia, Italy
[24a]INFN Sezione di Ferrara, I-44122, Ferrara, Italy
[24b]University of Ferrara, I-44122, Ferrara, Italy
[25]Institute of Physics and Technology, Peace Ave. 54B, Ulaanbaatar 13330, Mongolia
[26]Johannes Gutenberg University of Mainz, Johann-Joachim-Becher-Weg 45, D-55099 Mainz, Germany
[27]Joint Institute for Nuclear Research, 141980 Dubna, Moscow region, Russia
[28]Justus-Liebig-Universitaet Giessen, II. Physikalisches Institut,
Heinrich-Buff-Ring 16, D-35392 Giessen, Germany
[29]KVI-CART, University of Groningen, NL-9747 AA Groningen, Netherlands
[30]Lanzhou University, Lanzhou 730000, People's Republic of China
[31]Liaoning University, Shenyang 110036, People's Republic of China
[32]Nanjing Normal University, Nanjing 210023, People's Republic of China
[33]Nanjing University, Nanjing 210093, People's Republic of China
[34]Nankai University, Tianjin 300071, People's Republic of China
[35]Peking University, Beijing 100871, People's Republic of China
[36]Seoul National University, Seoul, 151-747 Korea
[37]Shandong University, Jinan 250100, People's Republic of China
[38]Shanghai Jiao Tong University, Shanghai 200240, People's Republic of China
[39]Shanxi University, Taiyuan 030006, People's Republic of China
[40]Sichuan University, Chengdu 610064, People's Republic of China
[41]Soochow University, Suzhou 215006, People's Republic of China
[42]Southeast University, Nanjing 211100, People's Republic of China
[43]State Key Laboratory of Particle Detection and Electronics,
Beijing 100049, Hefei 230026, People's Republic of China
[44]Sun Yat-Sen University, Guangzhou 510275, People's Republic of China
[45]Tsinghua University, Beijing 100084, People's Republic of China
[46a]Ankara University, 06100 Tandogan, Ankara, Turkey
[46b]Istanbul Bilgi University, 34060 Eyup, Istanbul, Turkey
[46c]Uludag University, 16059 Bursa, Turkey
[46d]Near East University, Nicosia, North Cyprus, Mersin 10, Turkey
[47]University of Chinese Academy of Sciences, Beijing 100049, People's Republic of China
[48]University of Hawaii, Honolulu, Hawaii 96822, USA
[49]University of Jinan, Jinan 250022, People's Republic of China
[50]University of Minnesota, Minneapolis, Minnesota 55455, USA
[51]University of Muenster, Wilhelm-Klemm-Str. 9, 48149 Muenster, Germany
[52]University of Science and Technology Liaoning, Anshan 114051, People's Republic of China
[53]University of Science and Technology of China, Hefei 230026, People's Republic of China

[54]University of South China, Hengyang 421001, People's Republic of China
[55]University of the Punjab, Lahore-54590, Pakistan
[56a]University of Turin, I-10125, Turin, Italy
[56b]University of Eastern Piedmont, I-15121, Alessandria, Italy
[56c]INFN, I-10125, Turin, Italy
[57]Uppsala University, Box 516, SE-75120 Uppsala, Sweden
[58]Wuhan University, Wuhan 430072, People's Republic of China
[59]Xinyang Normal University, Xinyang 464000, People's Republic of China
[60]Zhejiang University, Hangzhou 310027, People's Republic of China
[61]Zhengzhou University, Zhengzhou 450001, People's Republic of China

We report the observation and study of the decay $J/\psi \to \phi\eta\eta'$ using 1.3×10^9 J/ψ events collected with the BESIII detector. Its branching fraction, including all possible intermediate states, is measured to be $(2.32 \pm 0.06 \pm 0.16) \times 10^{-4}$. We also report evidence for a structure, denoted as X, in the $\phi\eta'$ mass spectrum in the 2.0–2.1 GeV/c^2 region. Using two decay modes of the η' meson ($\gamma\pi^+\pi^-$ and $\eta\pi^+\pi^-$), a simultaneous fit to the $\phi\eta'$ mass spectra is performed. Assuming the quantum numbers of the X to be $J^P = 1^-$, its significance is found to be 4.4σ, with a mass and width of $(2002.1 \pm 27.5 \pm 21.4)$ MeV/c^2 and $(129 \pm 17 \pm 9)$ MeV, respectively, and a product branching fraction $\mathcal{B}(J/\psi \to \eta X) \times \mathcal{B}(X \to \phi\eta') = (9.8 \pm 1.2 \pm 1.7) \times 10^{-5}$. Alternatively, assuming $J^P = 1^+$, the significance is 3.8σ, with a mass and width of $(2062.8 \pm 13.1 \pm 7.2)$ MeV/c^2 and $(177 \pm 36 \pm 35)$ MeV, respectively, and a product branching fraction $\mathcal{B}(J/\psi \to \eta X) \times \mathcal{B}(X \to \phi\eta') = (9.6 \pm 1.4 \pm 2.0) \times 10^{-5}$. The angular distribution of $J/\psi \to \eta X$ is studied and the two J^P assumptions of the X cannot be clearly distinguished due to the limited statistics. In all measurements the first uncertainties are statistical and the second systematic.

*Corresponding author.
longyf@pku.edu.cn
[a]Also at Bogazici University, 34342 Istanbul, Turkey.
[b]Also at the Moscow Institute of Physics and Technology, Moscow 141700, Russia.
[c]Also at the Functional Electronics Laboratory, Tomsk State University, Tomsk, 634050, Russia.
[d]Also at the Novosibirsk State University, Novosibirsk, 630090, Russia.
[e]Also at the NRC "Kurchatov Institute", PNPI, 188300, Gatchina, Russia.
[f]Also at Istanbul Arel University, 34295 Istanbul, Turkey.
[g]Also at Goethe University Frankfurt, 60323 Frankfurt am Main, Germany.
[h]Also at Key Laboratory for Particle Physics, Astrophysics and Cosmology, Ministry of Education; Shanghai Key Laboratory for Particle Physics and Cosmology; Institute of Nuclear and Particle Physics, Shanghai 200240, People's Republic of China.
[i]Government College Women University, Sialkot - 51310, Punjab, Pakistan.
[j]Key Laboratory of Nuclear Physics and Ion-beam Application (MOE) and Institute of Modern Physics, Fudan University, Shanghai 200443, People's Republic of China.
[k]Present address: Center for Underground Physics, Institute for Basic Science, Daejeon 34126, Korea.
[l]Also at State Key Laboratory of Nuclear Physics and Technology, Peking University, Beijing 100871, People's Republic of China.

I. INTRODUCTION

Exotic hadrons, e.g., glueballs, hybrid states and multi-quark states, are allowed in the framework of quantum chromodynamics (QCD), but no conclusive evidence for them has yet been found in the light hadron sector. The decay $J/\psi \to VPP$ (where V denotes vector and P denotes pseudoscalar) is an ideal probe to study light hadron spectroscopy and to search for new hadrons. There have been theoretical [1–4] and experimental [5–10] studies performed, which have mainly been focused on the V recoil system to search for exotic hadrons. The P recoil system, on the other hand, could also be utilized to do a similar study. For example, the $Y(2175)$, denoted as $\phi(2170)$ by the Particle Data Group (PDG) [11], was confirmed in the process $J/\psi \to \eta Y(2175)$, $Y(2175) \to \phi f_0(980)$ by BESII [12] and BESIII [13]. Searching for its decay to the $\phi\eta'$ state provides valuable input for understanding its nature [14]. The decay $J/\psi \to \phi\eta\eta'$ has not been studied before, and could aid in our understanding of J/ψ decay mechanisms and offers an opportunity to study possible intermediate states.

In this article, we report the observation and study of the decay $J/\psi \to \phi\eta\eta'$ using $(1310.6 \pm 7.0) \times 10^6$ J/ψ events [15] collected with the BESIII detector. Its branching fraction, including all possible intermediate states, is measured. We also report evidence for a structure denoted

as X in the $\phi\eta'$ mass spectrum in the 2.0–2.1 GeV/c^2 region. The mass and width of this structure, as well as the product branching fraction $\mathcal{B}(J/\psi \to \eta X) \times \mathcal{B}(X \to \phi\eta')$, are measured. The ϕ meson is reconstructed through its K^+K^- decay mode, η through $\gamma\gamma$, and η' through both $\gamma\pi^+\pi^-$ and $\eta\pi^+\pi^-$ (with the $\eta \to \gamma\gamma$), denoted as mode I and mode II, respectively.

II. BESIII EXPERIMENT AND MONTE CARLO SIMULATION

The BESIII detector is a magnetic spectrometer [16] located at the Beijing Electron Position Collider (BEPCII) [17]. The cylindrical core of the BESIII detector consists of a helium-based multilayer drift chamber (MDC), a plastic scintillator time-of-flight system (TOF), and a CsI(Tl) electromagnetic calorimeter (EMC), which are all enclosed in a superconducting solenoidal magnet providing a 1.0 T (0.9 T in 2012) magnetic field. The solenoid is supported by an octagonal flux-return yoke with resistive plate counter muon identifier modules interleaved with steel. The acceptance of charged particles and photons is 93% over 4π solid angle. The charged-particle momentum resolution at 1 GeV/c is 0.5%, and the dE/dx resolution is 6% for electrons from Bhabha scattering. The EMC measures photon energies with a resolution of 2.5% (5%) at 1 GeV in the barrel (end cap) region. The time resolution of the TOF barrel part is 68 ps, while that of the end cap part is 110 ps.

Simulated data samples produced with a GEANT4-based [18] Monte Carlo (MC) package, including the geometric description of the BESIII detector and the detector response, are used to determine the detection efficiency and to estimate the backgrounds. The simulation of the e^+e^- collisions includes the beam energy spread and initial state radiation (ISR) and is modeled using the generator KKMC [19]. The inclusive MC sample consists of the production of the J/ψ resonance and the continuum processes incorporated in KKMC [19]. The known decay modes are modeled with EVTGEN [20] using branching fractions taken from the PDG [11], and the remaining unknown decays from the charmonium states with LUNDCHARM [21]. Final state radiation (FSR) from charged final state particles is incorporated with the PHOTOS package [22].

III. EVENT SELECTION AND DATA ANALYSIS

Charged tracks are reconstructed from hits in the MDC. We select four charged tracks with net charge zero in the polar angle range $|\cos\theta| < 0.93$, and require their points of closest approach to the e^+e^- interaction point to be within ± 10 cm in the beam direction and 1 cm in the plane perpendicular to the beam direction. The dE/dx and TOF measurements are combined to form particle identification (PID) confidence levels for the π, K and p hypotheses. We require that one K^+K^- pair and one $\pi^+\pi^-$ pair are

identified. A vertex fit that assumes the $\pi^+\pi^-K^+K^-$ tracks all come from a common vertex is applied.

Photons are reconstructed from electromagnetic showers in the EMC. At least three photons are required for mode I and four for mode II. The minimum energy for showers to be identified as photons in the barrel region ($|\cos\theta| < 0.8$) is 25 MeV, and in the end caps ($0.86 < |\cos\theta| < 0.92$) is 50 MeV. Showers out of the above regions are poorly reconstructed and not used in this analysis. To suppress showers from charged particles, a photon must be separated by at least 10 degrees from the nearest charged track. EMC cluster timing requirements suppress electronic noise and energy deposits unrelated to this event.

Four-constraint (4C) kinematic fits are applied to all combinations of photons, and only the combination with the smallest χ^2_{4C} is kept. We only keep those events with $\chi^2_{4C} \leq 40$ for mode I and $\chi^2_{4C} \leq 80$ for mode II. To suppress background events containing π^0's, those events with the invariant mass of any photon pair within a π^0 mass window $[0.12 \leq M(\gamma\gamma) \leq 0.15$ GeV/$c^2]$ are rejected. For mode I, the combination with the smallest value of $\delta_1^2 = [M(\gamma_1\gamma_2) - m_\eta]^2/\sigma_\eta^2 + [M(\gamma_3\pi^+\pi^-) - m_{\eta'}]^2/\sigma_{\eta'}^2$ is used to assign photons to the η and η'. Here m_η and $m_{\eta'}$ are the nominal η and η' masses [11], respectively; σ_η and $\sigma_{\eta'}$ are the mass resolutions determined from signal MC simulation. Mass windows for the η, ϕ and η' mesons are (in GeV/c^2) $0.522 \leq M(\gamma\gamma) \leq 0.573$, $1.010 \leq M(K^+K^-) \leq 1.030$ and $0.936 \leq M(\gamma\pi^+\pi^-) \leq 0.979$. $M(\pi^+\pi^-)$ is required to be less than 0.87 GeV/c^2 to suppress the background from the $J/\psi \to \eta\phi f_0(980)$ process as shown in Fig. 1. For mode II, we use the combination with the smallest $\delta_2^2 = [M(\gamma_1\gamma_2) - m_\eta]^2/\sigma_\eta^2 + [M(\gamma_3\gamma_4) - m_\eta]^2/\sigma_\eta^2$ for the best η meson combination; the η for which $M(\pi^+\pi^-\eta)$ is closest to $m_{\eta'}$ is attributed to the candidate decaying from the η'. Mass windows for the η, ϕ and η' mesons are (in GeV/c^2) $0.509 \leq M(\gamma\gamma) \leq 0.586$, $1.010 \leq M(K^+K^-) \leq 1.030$ and $0.920 \leq M(\eta\pi^+\pi^-) \leq 0.995$.

Figure 2 shows the distributions of $M(\gamma\pi^+\pi^-)$ versus $M(K^+K^-)$ for mode I and $M(\eta\pi^+\pi^-)$ versus $M(K^+K^-)$ for mode II. The background inferred from the η sidebands is negligible according to both the study of the data and the corresponding inclusive MC samples for J/ψ decays. The non-ϕ and/or non-η' backgrounds are determined by the weighted sums of the horizontal and vertical sidebands with the entries in the diagonal sidebands subtracted to compensate for the double counting of background components. The different sidebands are illustrated in Fig. 2 and the weighting factors are obtained from the 2-dimensional (2D) fits to the mass spectra of $M(\gamma\pi^+\pi^-)$ versus $M(K^+K^-)$ and $M(\eta\pi^+\pi^-)$ versus $M(K^+K^-)$. The ϕ and η' meson signals are seen clearly in both modes. The three body decay $J/\psi \to \phi\eta\eta'$ is thus established, which is the first observation of this decay.
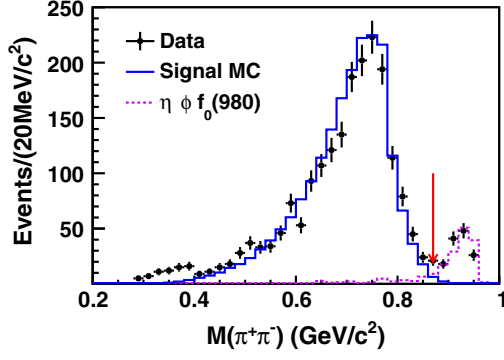
FIG. 1. The $M(\pi^+\pi^-)$ distribution for mode I, where dots with error bars are experimental data, the (blue) solid histogram shows the signal MC simulation, the (violet) dotted histogram shows the background from the $J/\psi \to \eta\phi f_0(980)$ process, and the arrow represents the mass requirement.

IV. MEASUREMENT OF $\mathcal{B}(J/\psi \to \phi\eta\eta')$

The branching fraction for $J/\psi \to \phi\eta\eta'$, including all possible intermediate states, is measured. Following the procedure in Ref. [23], the regions of $M^2(\phi\eta')$ versus $M^2(\phi\eta)$ are divided into 40×40 areas (each area is tagged by i and j) and the numbers of events (n_{data}^{ij}), non-ϕ and/or non-η' background (n_{bkg}^{ij}) and efficiency (ϵ_{ij}) are obtained individually in each area. Then $\mathcal{B}(J/\psi \to \phi\eta\eta')$ is determined by

$$\mathcal{B} = \frac{N_{\text{corr}}}{N_{J/\psi}\mathcal{B}(\eta \to 2\gamma)\mathcal{B}(\phi \to K^+K^-)\mathcal{B}_{\eta'}}, \quad (1)$$

where N_{corr} is the efficiency-corrected number of signal events and is determined from $N_{\text{corr}} = \Sigma_{ij}[(n_{\text{data}}^{ij} - n_{\text{bkg}}^{ij})/\epsilon_{ij}]$; $N_{J/\psi}$ is the total number of J/ψ events [15]; $\mathcal{B}$ is the PDG branching fraction [11]; $\mathcal{B}_{\eta'}$ is $\mathcal{B}(\eta' \to \gamma\pi^+\pi^-)$ for mode I and $\mathcal{B}(\eta' \to \eta\pi^+\pi^-) \times \mathcal{B}(\eta \to \gamma\gamma)$ for mode II. The total signal yield after background subtraction is 1684 ± 48 for mode I and 510 ± 25 for mode II; $\mathcal{B}(J/\psi \to \phi\eta\eta')$ is determined to be $(2.31 \pm 0.07) \times 10^{-4}$ for mode I and

TABLE I. Systematic uncertainties in $\mathcal{B}(J/\psi \to \phi\eta\eta')$. The correlated sources between the two η' decay modes are denoted with asterisks.

Sources	Mode I (%)	Mode II (%)
MDC tracking*	4.0	4.0
PID*	4.0	4.0
Photon detection*	1.8	2.4
Kinematic fit	2.5	1.1
Sideband regions	0.1	0.3
Mass window for η	0.5	0.7
Mass window for ϕ	0.9	1.0
Mass window for η'	0.7	0.6
MC statistics	0.6	0.9
Branching fractions*	2.1	2.1
Number of J/ψ*	0.6	0.6
2D binning	3.9	2.2
Total	8.0	7.2

$(2.34 \pm 0.12) \times 10^{-4}$ for mode II. The uncertainties are statistical only. The weighted average [24] of the results for the two η' decay modes is $(2.32 \pm 0.06 \pm 0.16) \times 10^{-4}$, after taking into account the correlations between uncertainties from the two modes, as denoted with asterisks in Table I.

The systematic uncertainties in $\mathcal{B}(J/\psi \to \phi\eta\eta')$ measurements are shown in Table I. The uncertainties from MDC tracking and PID efficiencies are established to be 1.0% per pion/kaon in Refs. [25,26]. The uncertainty related to photon detection is determined to be 0.6% per photon in Ref. [27]. The uncertainties associated with the 4C kinematic fit are studied with the track parameter correction method [28] and the differences between the efficiencies with and without corrections are regarded as uncertainties; the influence of the χ^2_{4C} requirement is also considered in the uncertainty determination. The sideband regions of the ϕ and η' mesons are shifted by 1σ (the nominal width of signal region corresponds to 3σ), and the effects on the results are assigned as uncertainties. The uncertainties from mass windows are determined by
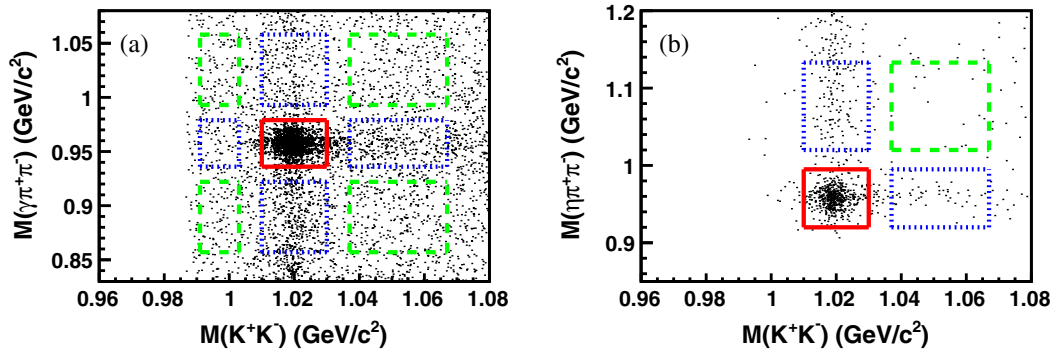

FIG. 2. Distributions of $M(\gamma\pi^+\pi^-)$ versus $M(K^+K^-)$ for mode I (a) and $M(\eta\pi^+\pi^-)$ versus $M(K^+K^-)$ for mode II (b), where the (red) solid rectangles show the signal regions; the (blue) dotted and (green) dashed rectangles represent the 2D sidebands.
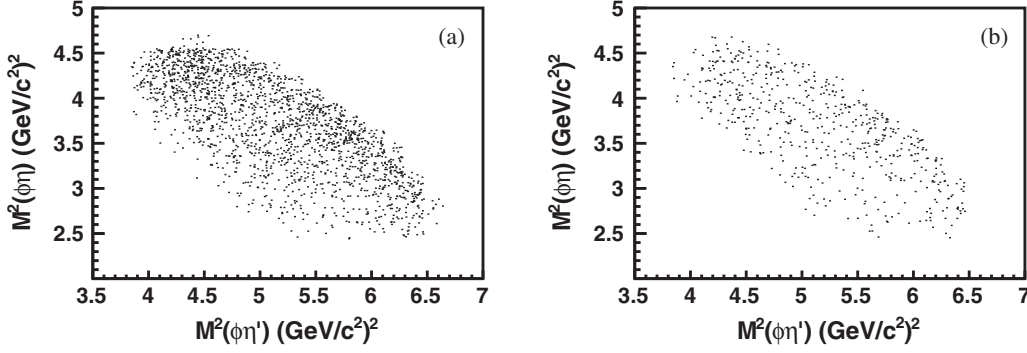
FIG. 3.   Dalitz plots for modes I (a) and II (b).

smearing the mass spectra from MC simulation to compensate for the differences between the resolutions from data and MC; the differences between efficiencies before and after smearing are taken as uncertainties. The influences of finite MC statistics are taken into account. The uncertainties due to quoted branching fractions and number of J/ψ events are from the PDG [11] and Ref. [15], respectively. The uncertainties from the 2D binning method are obtained by changing the numbers of areas in the $\mathcal{B}(J/\psi \to \phi\eta\eta')$ determination. The total systematic uncertainties are obtained by summing all contributions in quadrature, assuming they are independent.

V. STUDY OF AN INTERMEDIATE STATE IN THE $\phi\eta'$ MASS SPECTRUM

Figure 3 shows Dalitz plots for modes I and II. Both have concentrations of events with $M^2(\phi\eta')$ values near 4.5 $(\text{GeV}/c^2)^2$. There are also diagonal bands in both modes corresponding to the process $J/\psi \to \phi f_0(1500)$, $f_0(1500) \to \eta\eta'$ according to studies of the MC samples. Apart from these, no other structures are evident.

A. Simultaneous fit

With the assumption that there is an X structure in the $\phi\eta'$ mass spectrum in the 2.0–2.1 GeV/c^2 region, corresponding to the clusters near 4.5 $(\text{GeV}/c^2)^2$ visible in Fig. 3, a simultaneous fit is performed on the $\phi\eta'$ mass spectra for modes I and II. Since the spin-parity value (J^P) of the structure could affect the relative orbital angular momenta between the decay products of $J/\psi \to \eta X$ and $X \to \phi\eta'$, the fits with two different assumptions on the J^P value are both performed. However, due to the limited statistics, they cannot clearly be distinguished. In the simultaneous fits, the interference between the structure and the direct decay $J/\psi \to \phi\eta\eta'$ is not considered.

Assuming the J^P value of the structure to be 1^-, the signal component is parametrized by

$$\left(\left| \frac{1}{m^2 - M^2 + iM\Gamma/c^2} \right|^2 \times (pq)^3 \times \epsilon \right) \otimes R, \quad (2)$$

where m is the reconstructed mass of the $\phi\eta'$ system; M and Γ are the mass and width of the structure in the constant-width relativistic Breit-Wigner (BW) function; the P-wave phase space (PHSP) factor $(pq)^3$ is considered in the partial width, where p is the ϕ momentum in the $\phi\eta'$ rest frame, and q is the η momentum in the J/ψ rest frame; ϵ denotes the efficiency and R is the double-Gaussian resolution function, both of which are determined from a signal MC simulation. The mass and width of the BW function are allowed to float but are constrained to be the same for both modes; the signal ratio of the two modes is fixed based on PDG η' branching fractions [11] and MC-determined efficiencies. The total signal yield for the two modes is allowed to float in the fit. The background components consist of nonresonant $\phi\eta\eta'$, $J/\psi \to \phi f_0(1500)$, $f_0(1500) \to \eta\eta'$ and non-ϕ and/or non-η' processes. For the nonresonant $\phi\eta\eta'$ process, the line shapes are derived from the MC simulation of $J/\psi \to \phi\eta\eta'$ process generated according to PHSP, and the ratio of background numbers for the two modes is fixed, similar to the signal case. For $J/\psi \to \phi f_0(1500)$, $f_0(1500) \to \eta\eta'$ background, whose influence on the structure is small, the shapes are from MC simulation; $\mathcal{B}(J/\psi \to \phi f_0(1500)) \times \mathcal{B}(f_0(1500) \to \pi\pi)$ and $\mathcal{B}(J/\psi \to \phi f_0(1500)) \times \mathcal{B}(f_0(1500) \to K\bar{K})$ from BESII [9], together with $\mathcal{B}(f_0(1500) \to \pi\pi)$, $\mathcal{B}(f_0(1500) \to K\bar{K})$ and $\mathcal{B}(f_0(1500) \to \eta\eta')$ from the PDG [11], are used to obtain the expected number of $f_0(1500)$, and the background number is fixed to the expected value. The non-ϕ and/or non-η' backgrounds are determined from the 2D sidebands of the ϕ and η' mesons as shown in Fig. 2.

Figure 4 shows the results of the simultaneous fit, where the mass and width of the structure are determined to be (2002.1 ± 27.5) MeV/c^2 and (129 ± 17) MeV, respectively. The log-likelihood value is 15591.8, with a goodness-of-fit value of χ^2/d.o.f. of $20.98/26 = 0.81$ for mode I and $25.97/26 = 1.00$ for mode II. The statistical significance of the new structure is calculated to be larger than 10σ, determined from the change of the log-likelihood values and the numbers of free parameters in the fits with and without the inclusion of the structure. After smearing the likelihood curve with the Gaussian-distributed
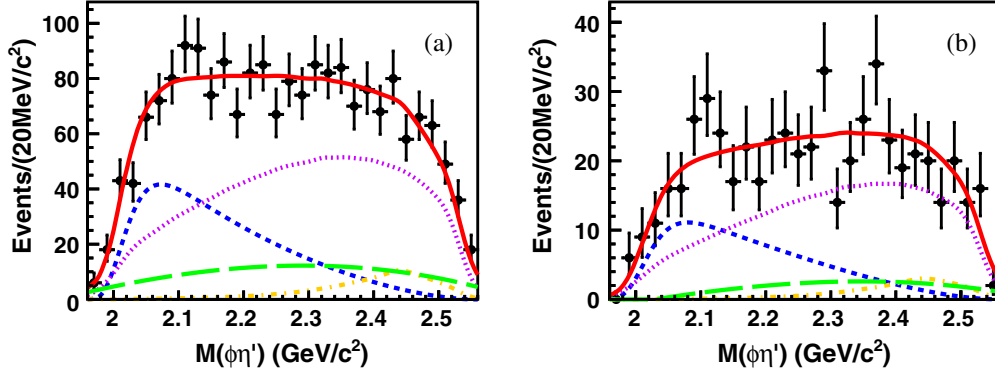
FIG. 4. Results of the simultaneous fit with the 1^- assumption for modes I (a) and II (b). Dots with error bars are experimental data and the (red) solid curves show the fit model. The (blue) dashed curves are the signal component. The (violet) dotted curves show the background from the $J/\psi \to \phi\eta\eta'$ PHSP process. The (orange) dot-dashed curves represent the background from the $J/\psi \to \phi f_0(1500)$, $f_0(1500) \to \eta\eta'$ process. The (green) long-dashed curves show the non-ϕ and/or non-η' backgrounds.

systematic uncertainties (Table III), the significance is evaluated to be 4.4σ. Many checks have been done to make sure that none of the possible background contributions could produce peaking backgrounds in the 2.0–2.1 GeV/c^2 region in the $\phi\eta'$ mass spectrum. A comparison between data and MC also indicates no significant structures in the $\phi\eta$ mass spectrum.

Assuming the J^P value of the structure to be 1^+, the simultaneous fit with the S-wave PHSP factor pq in the partial width is performed with results shown in Fig. 5. The mass and width of the structure are determined to be (2062.8 ± 13.1) MeV/c^2 and (177 ± 36) MeV, respectively. The log-likelihood value is 15595.9, with a goodness-of-fit value of $\chi^2/\text{d.o.f.}$ of $16.68/26 = 0.64$ for mode I and $24.36/26 = 0.94$ for mode II. The significance of the structure after considering the systematic uncertainties (Table IV) is evaluated to be 3.8σ.

B. Angular distribution

The J^P assignment for the structure is investigated by examining the distribution of $|\cos\theta|$, where θ is the η polar angle in the J/ψ rest frame. If $J^P = 1^-$, the decay $J/\psi \to \eta X$ takes place through a P wave, neglecting the higher orbital angular momenta due to the closeness of the threshold, and the $|\cos\theta|$ is expected to follow a $1 + \cos^2\theta$ distribution. If $J^P = 1^+$, the above decay takes place through an S wave, where the $|\cos\theta|$ distribution is expected to be flat.

The events are divided into four intervals of $|\cos\theta|$, and the total signal yield in each interval is obtained with the same simultaneous fit method with a 1^+ assumption, as described above. After efficiency correction and normalization, the $|\cos\theta|$ distribution of data is shown in Fig. 6, together with the fitting results with the 1^- and 1^+ assumptions. The 1^- assumption has $\chi^2/\text{d.o.f.}$ value being $10.55/3 = 3.52$ while for the 1^+ assumption it is $4.41/3 = 1.47$. Although the $\chi^2/\text{d.o.f.}$ value favors the 1^+ assumption, these two assumptions cannot clearly be distinguished due to the limited statistics. The 0^+ assumption is ruled out because it violates J^P conservation, and the 0^- assumption is rejected at 99.5% confidence level from the Pearson χ^2 test. The results of simultaneous fit with 1^- assumption are consistent with those from 1^+.
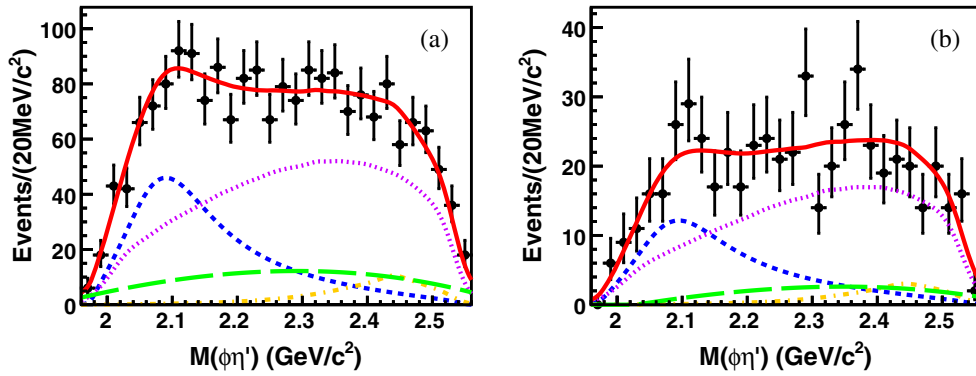

FIG. 5. Results of the simultaneous fit with the 1^+ assumption for modes I (a) and II (b). Dots with error bars are experimental data and the (red) solid curves show the fit model. The (blue) dashed curves are the signal component. The (violet) dotted curves show the background from the $J/\psi \to \phi\eta\eta'$ PHSP process. The (orange) dot-dashed curves represent the background from the $J/\psi \to \phi f_0(1500)$, $f_0(1500) \to \eta\eta'$ process. The (green) long-dashed curves show the non-ϕ and/or non-η' backgrounds.
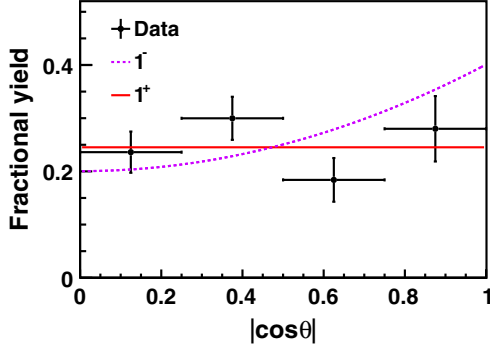
FIG. 6.   Distribution of the η polar angle in the J/ψ rest frame. Dots with error bars are experimental data. The (violet) dashed curve is the fitting result with the 1^- assumption, and the (red) solid curve is that with the 1^+ assumption.

C. Measurement of the product branching fraction

The product branching fraction to the $\eta\phi\eta'$ final state via X is

$$\mathcal{B}(J/\psi \to \eta X) \times \mathcal{B}(X \to \phi\eta')$$
$$= \frac{N_{\text{sig}}}{N_{J/\psi}\mathcal{B}(\eta \to 2\gamma)\mathcal{B}(\phi \to K^+K^-)\bar{\epsilon}}, \quad (3)$$

where N_{sig} is the total signal yield from the two modes in the simultaneous fit; $\bar{\epsilon}$ is $\mathcal{B}(\eta' \to \gamma\pi^+\pi^-)\epsilon_{\text{I}} + \mathcal{B}(\eta' \to \eta\pi^+\pi^-)\mathcal{B}(\eta \to 2\gamma)\epsilon_{\text{II}}$, where ϵ_{I} and ϵ_{II} are the detection efficiencies determined from signal MC simulation after considering the J^P value of the structure and the angular distributions of the η, ϕ and η'; the other variables have been defined before. The measured N_{sig} and $\mathcal{B}(J/\psi \to \eta X) \times \mathcal{B}(X \to \phi\eta')$ values for the 1^- and 1^+ assumptions are summarized in Table II, where the uncertainties are statistical only.

D. Systematic uncertainties

Tables III and IV summarize the systematic uncertainties in the measurements of mass and width of the structure, as well as $\mathcal{B}(J/\psi \to \eta X) \times \mathcal{B}(X \to \phi\eta')$ for the 1^- and 1^+ assumptions, respectively. In case there are differences between the uncertainties from the two modes, the more conservative values are used.

The signal parametrization is changed from a constant-width BW function to a BW with mass-dependent width. The impact on the signal yield is taken as the uncertainty of $\mathcal{B}(J/\psi \to \eta X) \times \mathcal{B}(X \to \phi\eta')$. The pole mass ($m_{\text{pole}}$) and

TABLE II.   Measured N_{sig} and $\mathcal{B}(J/\psi \to \eta X) \times \mathcal{B}(X \to \phi\eta')$ values for the 1^- and 1^+ assumptions.

J^P	N_{sig}	$\mathcal{B}(J/\psi \to \eta X) \times \mathcal{B}(X \to \phi\eta')$
1^-	658 ± 77	$(9.8 \pm 1.2) \times 10^{-5}$
1^+	642 ± 88	$(9.6 \pm 1.4) \times 10^{-5}$

TABLE III.   Systematic uncertainties in the mass and width of the structure, as well as $\mathcal{B}(J/\psi \to \eta X) \times \mathcal{B}(X \to \phi\eta')$ (denoted as $\mathcal{B}_X$ in this table) for the 1^- assumption.

Sources	Mass (MeV/c^2)	Width (MeV)	$\mathcal{B}_X$ (%)
Signal parametrization	9.1	2	2.9
$f_0(1500)$	9.5	5	11.6
PHSP assumption	15.2	5	9.8
Fitting range	6.3	3	3.1
$M(\pi^+\pi^-)$ requirement	1.8	2	0
Extra structures	2.5	0	1.1
Momentum calibration	0.7	$\cdots$	$\cdots$
Sideband regions	0.9	2	0.4
MDC tracking	$\cdots$	$\cdots$	4.0
PID	$\cdots$	$\cdots$	4.0
Photon detection	$\cdots$	$\cdots$	2.4
Kinematic fit	$\cdots$	$\cdots$	3.0
Mass window for η	$\cdots$	$\cdots$	0.7
Mass window for ϕ	$\cdots$	$\cdots$	1.0
Mass window for η'	$\cdots$	$\cdots$	0.7
MC statistics	$\cdots$	$\cdots$	0.9
Branching fractions	$\cdots$	$\cdots$	2.1
Number of J/ψ	$\cdots$	$\cdots$	0.6
Total	21.4	9	17.5

pole width (Γ_{pole}) are obtained by solving for the complex equation $P = m_{\text{pole}} - i\Gamma_{\text{pole}}/2$ for which the BW denominator is zero, and the differences between the mass and width from the nominal fit and m_{pole} and Γ_{pole} are considered as the uncertainties of mass and width, respectively. To obtain the uncertainties associated with the $f_0(1500)$ component of the data, the background levels in the simultaneous fit are varied by $\pm 1\sigma$ [9,11], where σ denotes the uncertainty on the determined number of the $f_0(1500)$, and the maximum changes in the fit results are regarded as uncertainties. We also vary the nonresonant $\phi\eta'$ background levels by $\pm 1\sigma$, and take the largest influences on the fit results as the uncertainties due to the PHSP assumption. We vary the range of the simultaneous fit by 5% and take the largest deviations of the fitting results as uncertainties. To obtain the uncertainties due to the $M(\pi^+\pi^-)$ requirement for mode I, it is relaxed from 0.87 to 0.90 GeV/c^2 and the effects on the fitting results are considered as uncertainties. The two possible extra structures around 2.3 GeV/c^2 in Figs. 4(b) and 5(b) are considered. Following the procedure in Ref. [13], we use BW functions convolved with a resolution function to describe them and the corresponding significances are determined to be less than 1.1σ, and they are not considered in the nominal result. However, their impacts on the fitting results are taken as systematic uncertainties. The difference between the fitted η mass and that from the PDG [11] is taken as the uncertainty due to momentum calibration. The descriptions of other items are included in Table I. The total

TABLE IV. Systematic uncertainties in the mass and width of the structure, as well as $\mathcal{B}(J/\psi \to \eta X) \times \mathcal{B}(X \to \phi\eta')$ (denoted as $\mathcal{B}_X$ in this table) for the 1^+ assumption.

Sources	Mass (MeV/c^2)	Width (MeV)	$\mathcal{B}_X$ (%)
Signal parametrization	2.4	0	0.4
$f_0(1500)$	2.6	19	13.4
PHSP assumption	5.9	28	12.4
Fitting range	1.1	6	3.2
$M(\pi^+\pi^-)$ requirement	1.3	1	0
Extra structures	0.7	1	1.9
Momentum calibration	0.7	$\cdots$	$\cdots$
Sideband regions	0.7	1	0.4
MDC tracking	$\cdots$	$\cdots$	4.0
PID	$\cdots$	$\cdots$	4.0
Photon detection	$\cdots$	$\cdots$	2.4
Kinematic fit	$\cdots$	$\cdots$	2.3
Mass window for η	$\cdots$	$\cdots$	0.7
Mass window for ϕ	$\cdots$	$\cdots$	1.0
Mass window for η'	$\cdots$	$\cdots$	0.7
MC statistics	$\cdots$	$\cdots$	0.9
Branching fractions	$\cdots$	$\cdots$	2.1
Number of J/ψ	$\cdots$	$\cdots$	0.6
Total	7.2	35	20.0

systematic uncertainties are the quadrature sums of the individual contributions, assuming they are independent.

VI. SUMMARY AND DISCUSSION

In summary, using $(1310.6 \pm 7.0) \times 10^6$ J/ψ events collected with the BESIII detector, we report the observation and study of the process $J/\psi \to \phi\eta\eta'$. Its branching fraction, including all possible intermediate states, is determined to be $(2.32 \pm 0.06 \pm 0.16) \times 10^{-4}$. Evidence for a structure denoted as X in the $\phi\eta'$ mass spectra in two dominant η' decay modes is reported, and a simultaneous fit is performed. Assuming the J^P value of the structure to be 1^-, the significance of the structure is evaluated to be 4.4σ; the mass and width are determined to be $(2002.1 \pm 27.5 \pm 21.4)$ MeV/c^2 and $(129 \pm 17 \pm 9)$ MeV, respectively; the product branching fraction $\mathcal{B}(J/\psi \to \eta X) \times \mathcal{B}(X \to \phi\eta')$ is measured to be $(9.8 \pm 1.2 \pm 1.7) \times 10^{-5}$. The mass of the structure is over 5σ away from that of the $Y(2175)$ in the PDG [11], suggesting the structure might not be the

$Y(2175)$. For a 1^+ assumption, the significance is evaluated to be 3.8σ; the mass and width are determined to be $(2062.8 \pm 13.1 \pm 7.2)$ MeV/c^2 and $(177 \pm 36 \pm 35)$ MeV, respectively; the product branching fraction $\mathcal{B}(J/\psi \to \eta X) \times \mathcal{B}(X \to \phi\eta')$ is measured to be $(9.6 \pm 1.4 \pm 2.0) \times 10^{-5}$. The angular distribution is studied and the 1^- and 1^+ assumptions cannot clearly be distinguished due to the limited statistics. No meson candidate in the PDG has mass, width and J^P values that are compatible with the structure. More studies with a larger J/ψ data sample in the future might help to better understand the structure, including a J^P determination and precise measurements of the mass, width, and product branching fraction.

[1] D. Morgan and M. R. Pennington, Phys. Rev. D **48**, 5422 (1993).

[2] U. G. Meissner and J. A. Oller, Nucl. Phys. **A679**, 671 (2001); L. Roca, J. E. Palomar, E. Oset, and H. C. Chiang, Nucl. Phys. **A744**, 127 (2004); T. A. Lahde and U. G. Meissner, Phys. Rev. D **74**, 034021 (2006).

[3] B. Liu, M. Buescher, F. K. Guo, C. Hanhart, and U. G. Meissner, Eur. Phys. J. C **63**, 93 (2009).

[4] P. Chatzis, A. Faessler, T. Gutsche, and V. E. Lyubovitskij, Phys. Rev. D **84**, 034027 (2011).

[5] W. S. Lockman, AIP Conf. Proc. **150**, 776 (1986).

[6] A. Falvard *et al.* (DM2 Collaboration), Phys. Rev. D **38**, 2706 (1988).

[7] M. Ablikim *et al.* (BES Collaboration), Phys. Lett. B **598**, 149 (2004).

[8] M. Ablikim *et al.* (BES Collaboration), Phys. Lett. B **603**, 138 (2004).

[9] M. Ablikim *et al.* (BES Collaboration), Phys. Lett. B **607**, 243 (2005).

[10] M. Ablikim *et al.* (BES Collaboration), Phys. Lett. B **633**, 681 (2006).

[11] M. Tanabashi *et al.* (Particle Data Group), Phys. Rev. D **98**, 030001 (2018).

[12] M. Ablikim *et al.* (BES Collaboration), Phys. Rev. Lett. **100**, 102003 (2008).

[13] M. Ablikim *et al.* (BESIII Collaboration), Phys. Rev. D **91**, 052017 (2015).

[14] G. J. Ding and M. L. Yan, Phys. Lett. B **650**, 390 (2007).

[15] M. Ablikim *et al.* (BESIII Collaboration), Chin. Phys. C **41**, 013001 (2017).

[16] M. Ablikim *et al.* (BESIII Collaboration), Nucl. Instrum. Methods Phys. Res., Sect. A **614**, 345 (2010).

[17] C. H. Yu *et al.*, *Proceedings of IPAC2016, Busan, Korea* (JACoW, Geneva, Switzerland, 2016), http://dx.doi.org/10.18429/JACoW-IPAC2016-TUYA01.

[18] S. Agostinelli *et al.* (GEANT4 Collaboration), Nucl. Instrum. Methods Phys. Res., Sect. A **506**, 250 (2003).

[19] S. Jadach, B. F. L. Ward, and Z. Was, Comput. Phys. Commun. **130**, 260 (2000); Phys. Rev. D **63**, 113009 (2001).

[20] D. J. Lange, Nucl. Instrum. Methods Phys. Res., Sect. A **462**, 152 (2001); R. G. Ping, Chin. Phys. C **32**, 599 (2008).

[21] J. C. Chen, G. S. Huang, X. R. Qi, D. H. Zhang, and Y. S. Zhu, Phys. Rev. D **62**, 034003 (2000); R. L. Yang, R. G. Ping, and H. Chen, Chin. Phys. Lett. **31**, 061301 (2014).

[22] E. Richter-Was, Phys. Lett. B **303**, 163 (1993).

[23] M. Ablikim *et al.* (BESIII Collaboration), Phys. Rev. D **87**, 012007 (2013).

[24] G. D'Agostini, Nucl. Instrum. Methods Phys. Res., Sect. A **346**, 306 (1994).

[25] M. Ablikim *et al.* (BESIII Collaboration), Phys. Rev. Lett. **107**, 092001 (2011).

[26] M. Ablikim *et al.* (BESIII Collaboration), Phys. Rev. D **83**, 112005 (2011).

[27] M. Ablikim *et al.* (BESIII Collaboration), Phys. Rev. D **96**, 112012 (2017).

[28] M. Ablikim *et al.* (BESIII Collaboration), Phys. Rev. D **87**, 012002 (2013).